

# A Composite Neuronal System as Miniaturized Visual Modality for Collision Perception \*

Mengying Wang<sup>1,2</sup>, Jiajun Huang<sup>1,2</sup>, Xuelong Sun<sup>1,2</sup>, Cheng Hu<sup>2,3</sup>, Jigen Peng<sup>1,2</sup>, and Qinbing Fu<sup>1,2,\*</sup>

<sup>1</sup> School of Mathematics and Information Science, Guangzhou University, China

<sup>2</sup> Machine Life and Intelligence Research Centre, Guangzhou University, China

<sup>3</sup> School of Mechanical and Electrical Engineering, Guangzhou University, China

**Abstract.** Collision perception is a critical capability for intelligent mobile robots. Recent advancements in neural modeling have demonstrated that a composite neuron model, inspired by the Lobula Giant Movement Detectors (LGMDs) in locusts, offers enhanced collision selectivity by specifically responding to approaching targets. This characteristic shows great promise for improving robot collision detection as a sensor strategy. However, the model's significant computational demands in terms of time and memory have hindered its application in robots with extremely limited computational resources. To address this problem, this paper introduces an optimized online collision perception visual system designed for a ground-based miniaturized robot. The system enhances the existing composite neuronal model by simplifying network structures and optimizing spatiotemporal functions. It has been implemented on a micro-robot equipped with an STM32F427 chip, with a diameter of approximately 4 cm and a weight of 50 g. The visual system efficiently processes continuous image streams at over 80 Hz while utilizing only 176 KB of memory. Arena tests have confirmed the system's effectiveness and robustness in rapid collision detection, achieving a success ratio of 98.5%. Additionally, the results demonstrate the proposed model's improved selectivity in handling high-speed motion stimuli, responding exclusively to approaching movements rather than receding or translating ones. This study offers a robust and parsimonious solution for mobile robots with constrained visual computing resources, effectively addressing the challenge of collision perception.

**Keywords:** bio-inspired, composite neuronal model, embedded visual module, collision perception, collision selectivity, parsimony

---

\* Supported by the National Natural Science Foundation of China under Grants No. 12031003, 62376063, 62206066, 52202492, the Social Science Fund of the Ministry of Education of China under Grant No. 22YJCZH032, the International Cooperation and Exchange Project, NSFC-PSF, No. 12211540710. \*Corresponding author: Qinbing Fu ([qifu@gzhu.edu.cn](mailto:qifu@gzhu.edu.cn)).

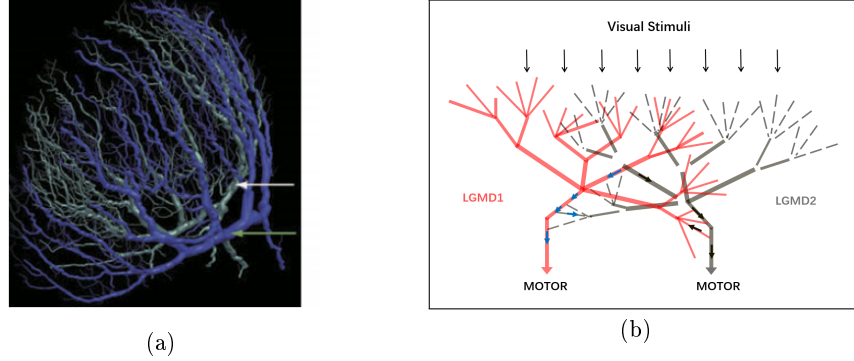


**Fig. 1:** (a) Neuromorphology: 3D reconstruction of the dendrites of two neighboring neurons, LGMD1 (indicated by the white arrow) and LGMD2 (indicated by the green arrow), image courtesy of [17]. (b) Schematic illustration of signal transmission between dendritic areas of LGMD1 and LGMD2, based on our assumption of two composite forms.

## 1 Introduction

The ability to detect collisions is crucial for mobile robotics, particularly when operating in complex, dynamic, and unpredictable environments. Various sensing modalities, such as laser, radar, infrared, ultrasound, and vision, have been employed for collision detection [10,7]. Among these, vision-based systems are particularly appealing because they can extract rich visual features from the environment, enabling the recognition of targets in real-time. However, the primary challenge with visual systems lies in their reliance on methods such as learning, segmentation, or registration [2], which typically require substantial computational power and large memory capacity. Consequently, these systems are often unsuitable for small or miniature robots with extremely limited computational resources. This raises the question: is there a more efficient way to utilize vision for robust collision detection?

The natural world continually surprises us with powerful resources, particularly in biological visual systems, which offer abundant inspiration for developing artificial vision systems. Notably, many bio-inspired models have been constructed based on the visual neural networks of insects [3,15,4]. These bio-inspired methods possess several advantages: (1) simplicity and efficiency, as they rely on low-level image processing; (2) low energy consumption, due to their simpler processing methods; and (3) high-speed processing, capable of operating on microsecond to millisecond timescales, making them suitable for real-time applications. These advantages have enabled successful implementation in robotics, such as optic flow-based collision avoidance strategies in micro-aerial vehicles [15], collision avoidance models inspired by the Lobula Giant Motion Detector (LGMD) in ground mobile robots [6,18], and navigation models based on the bee's visual "odometer" using the Elementary Motion Detector (EMD) in flying robots [9,14].

However, current single-neuron computational models continue to face significant challenges in real-world scenarios, particularly in terms of robustness and selectivity in robotic applications. For instance, the neural structures of LGMD1 and LGMD2 within the locust's visual systems are highly effective at detecting

looming objects and triggering escape behaviors [13,16]. Despite being adjacent to each other and sharing similar physiological characteristics (Figure 1), these neurons exhibit distinct selectivity: LGMD1 responds to both darker and brighter approaching objects, whereas LGMD2 specifically responds to darker approaching objects. Nevertheless, these neuronal models have two major limitations: first, they struggle to respond promptly to high-speed approaching objects, particularly in complex and dynamically changing environments, leading to ineffective collision avoidance; second, they often misidentify translating and receding stimuli as potential collisions. Thus, more reliable and effective methods are required to address these shortcomings.

To enhance the selectivity of bio-inspired collision detection techniques, Li et al. expanded the forward dendritic circuitry of existing LGMD models and proposed a composite model with two configurations: LGMD1-LGMD2 and LGMD2-LGMD1 [12]. In the LGMD1-LGMD2 configuration, the output of the presynaptic neuropil of LGMD1 serves as input for the dendritic computation of LGMD2, while in the LGMD2-LGMD1 configuration, the roles are reversed (Figure 1). This study demonstrated that incorporating the dendritic computations of these two neurons can mutually enhance each other’s collision selectivity, effectively mitigating the effects of translating and receding stimuli, closely mirroring phenomena observed in organisms. Moreover, the composite neuronal model shows superior adaptation to complex and dynamic environments compared to single-neuron computational models.

While the composite neuronal model significantly enhances collision selectivity, making it ideal for vision modules in ground mobile robots, transferring these models to embedded vision systems poses substantial challenges. Taking the *Colias* robot [8] used in this study as an example, embedded vision systems are limited by constrained computational resources, with a total SRAM capacity of 256KB and a requirement to process data within 33ms to ensure real-time performance. Previous implementations of LGMD1 and LGMD2 embedded vision systems occupy approximately 149KB and 157KB of memory, respectively, with the composite system estimated to require around 306KB of memory when combined in a straightforward manner. Thus, optimizing the composite system’s memory usage to stay within the required limits is a significant challenge. Additionally, each individual system takes approximately 24ms to process, and the increased computational complexity of the composite system could potentially exceed the 33ms limit, thereby compromising real-time performance.

In this paper, we aimed to integrate the composite neuronal model into the vision module of the *Colias* robot to develop a bio-inspired embedded collision detection system that maintains the robustness and selectivity of the corresponding offline model. To achieve this, we restructured the neural network of the composite model and optimized its memory usage and computational efficiency. The proposed model now occupies only 176KB of memory and requires just 12ms of processing time. We validated the feasibility of this system through a series of online experiments using multiple *Colias* robots. The results demonstrated not only the efficacy and robustness of this method as a miniaturized visual

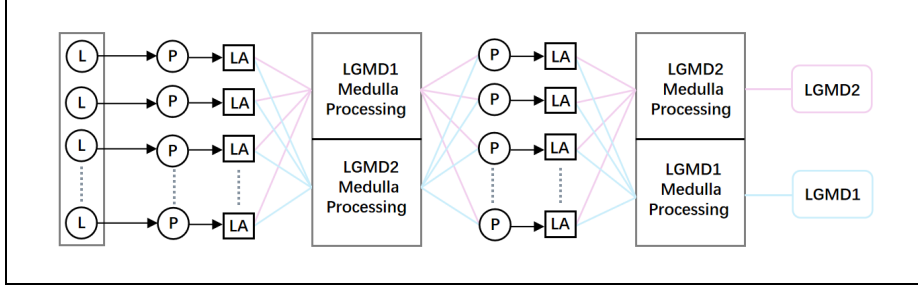


**Fig. 2:** The schematic illustration of the proposed composite LGMDs neuronal model depicts two forms of signal processing: the pink flow represents the LGMD1-LGMD2 configuration, while the blue flow represents LGMD2-LGMD1. The input consists of image streams at gray-scale luminance ( $L$ ), arranged in a matrix and captured by photoreceptors (P). LA denotes the Lamina layer, which is presynaptic to the LGMDs. The neural computation within the Medulla layer differs between LGMD1 and LGMD2, contributing to the distinct processing pathways in each configuration.

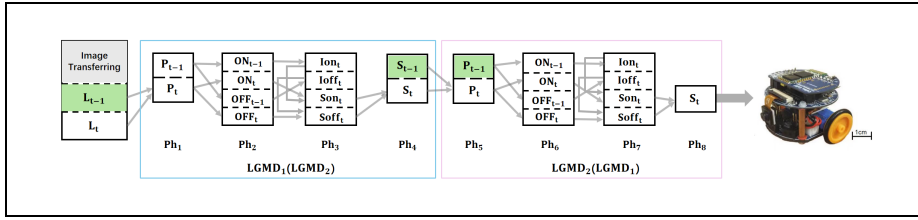


**Fig. 3:** The visual processing pipeline in embedded vision consists of eight phases (Ph) at frame- $t$ . The blue box represents the first module of the composite neuronal model, while the pink box represents the second module. In the case of LGMD1-LGMD2, LGMD1 serves as the first module, and LGMD2 serves as the second module, with the roles reversed in the opposite configuration. It is important to note that visual processing at the photoreceptor and inhibitory unit levels relies on delayed information stored in the memory.

modality with constrained resources for real-world visual processing but also its superior performance in detecting high-speed approaching objects, thanks to the deepened neural network framework.

The remainder of this paper is organized as follows: Section 2 details the optimized composite neuronal model; Section 3 presents experimental results and analysis; and Section 4 provides a summary and discusses future work.

## 2 Methods and Materials

In this section, we present the specific algorithm of the proposed composite LGMDs neuronal model, as well as the configuration and materials.

### 2.1 The Proposed Composite Neuronal Model

The composite neuronal model used in this paper builds upon the previous models proposed by Li et al. with more details in [12], as illustrated in Figure 2. We herein only showcase the key changes of algorithms for optimization. The earlier

models faced limitations due to excessive computational and memory requirements, which exceeded the capacity of embedded microprocessors, making them unsuitable for micro-robots. To overcome this issue, we focused on optimizing the Lamina and Medulla layers of the models. The following outline the key optimizations:

First, the Lamina layer comprises ON/OFF-type cells that receive visual motion information  $M(x, y, t)$  from the photoreceptors, capturing both luminance increases and decreases (luminance changes can be considered a specific form of motion). ON cells transmit luminance increases through the ON pathway, while OFF cells transmit luminance decreases through the OFF pathway, each processed via the ON/OFF mechanism [4]. In the earlier model [12], the Lamina layer is defined as

$$P_{ON}^k(x, y, t) = [M^k(x, y, t)]^+ + \beta \cdot P_{ON}^k(x, y, t - 1),$$

$$P_{OFF}^k(x, y, t) = -[M^k(x, y, t)]^- + \beta \cdot P_{OFF}^k(x, y, t - 1),$$

where  $[x]^+$  and  $[x]^-$  denote  $\max(0, x)$  and  $\min(x, 0)$ , and  $\beta$  denotes a delay coefficient, which represents the fraction of the previous signal allowed to pass. The superscript  $k \in \{1, 2\}$  denotes the type of neuron, including LGMD1 (1) and LGMD2 (2). To reduce computational complexity, we have implemented the following optimizations on temporal dimension of ON/OFF-type cell matrices:

$$P_{ON}^k(x, y, t) = [M^k(x, y, t)]^+, \quad P_{OFF}^k(x, y, t) = -[M^k(x, y, t)]^-. \quad (1)$$

In the previous formula, the values of  $P_{ON}^k(x, y, t)$  and  $P_{OFF}^k(x, y, t)$  depend on the information of the previous frame and the delay coefficient  $\beta$ , this dependence introduced additional multiplication operation, resulting in increased computational complexity. While in Eq. 1, the multiplication operation is removed, which simplifies the computational logic and thus reduces the computational complexity to some extent.

Second, the Medulla layer processes the output from the Lamina layer, further handling visual information by incorporating competition between excitatory and inhibitory flows, which is crucial for the model's collision selectivity. In the earlier model, local excitation  $E_{ON}^k$  and  $E_{OFF}^k$  in the ON and OFF pathways were derived through convolution operations on  $P_{ON}^k$  and  $P_{OFF}^k$ , respectively, using a convolution kernel with a radius of 1 and a uniform distribution. Peripheral delayed excitation  $D_{ON}^k$  and  $D_{OFF}^k$  were obtained via first-order low-pass filtering, followed by convolution to compute local inhibition  $I_{ON}^k$  and  $I_{OFF}^k$  in the respective pathways. The details are as follows:

$$D^k(t) = (E^k(t), D^k(t - 1), D^k(t - 2)) \cdot \vec{\alpha}^k,$$

$$I^k(x, y, t) = \sum_{i=-2}^2 \sum_{j=-2}^2 D^k(x + i, y + j, t) W^k(i + 1, j + 1).$$

Here,  $\vec{\alpha}^k$  denotes the delay coefficient, and  $W^k$  represents the convolution kernel used to obtain inhibition, specifically  $W_{I_{on}}^k$  and  $W_{I_{off}}^k$  for the two pathways,

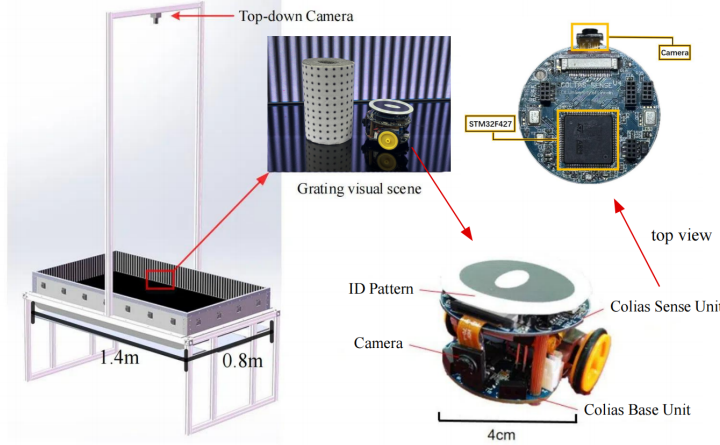


Fig. 4: Illustration of the arena and the ground-based micro-robot *Colias*, equipped with a visual module.

respectively, as follows:

$$[W_{I_{off}}^k] = \frac{1}{16} \begin{bmatrix} 1 & 2 & 4 & 2 & 1 \\ 2 & 4 & 8 & 4 & 2 \\ 4 & 8 & 16 & 8 & 4 \\ 1 & 2 & 4 & 2 & 1 \\ 2 & 4 & 8 & 4 & 2 \end{bmatrix}, [W_{I_{on}}^1] = [W_{I_{off}}^2], [W_{I_{on}}^2] = 2 * [W_{I_{off}}^2].$$

After optimizing the model, the outputs from the Lamina layer are directly fed into the corresponding E layers in the ON/OFF pathways to obtain local excitation. This approach eliminates convolution operations, which reduces a large number of multiplication and addition operations, thereby improving the computational efficiency of the model and shortening the overall running time. During real-time collision detection tasks, the robot can retain information from the previous frame (i.e.,  $t-1$ ) but not from  $t-2$ . Consequently, local inhibition is derived by performing convolution operations on  $P_{ON}^k$  and  $P_{OFF}^k$  from the previous frame. This approach not only reduces computational complexity but also conserves memory by eliminating the need for additional storage for peripheral delayed excitation. The entire spatiotemporal process is defined as follows:

$$I^k(x, y, t) = \sum_{i=-1}^1 \sum_{j=-1}^1 P^k(x+i, y+j, t-1) W^k(i+1, j+1). \quad (2)$$

Moreover, a convolution kernel with a radius of 2 can cover more input pixels and is effective at capturing more precisely the features of approaching objects. However, it requires more memory to store its data and intermediate results, leading to increased memory usage and a higher number of multiplication and addition operations for the convolution process. Additionally, handling boundary pixel points becomes more complex with a larger radius. In contrast, a convolution kernel with a radius of 1 not only uses less memory but also allows for direct bit operations on  $P_{ON}^k$  and  $P_{OFF}^k$  to compute local inhibition. This avoids the need for multiplication and division operations, significantly enhancing computational efficiency in embedded system. Therefore, the convolution kernel has

Table 1: Setting the key parameters

| Parameter(in Eq.) | Description                    | Value |
|-------------------|--------------------------------|-------|
| $\alpha$ (Eq. 4)  | scale parameter of firing rate | 4     |
| $T_{spi}$ (Eq. 4) | spiking threshold              | 0.7   |
| $n_{sp}$ (Eq. 5)  | number of successive spikes    | 5     |

Table 2: *Colias* robot configuration

|                       |                          |
|-----------------------|--------------------------|
| Dimensions            | $\phi$ 40 x $h$ 32 mm    |
| SRAM                  | 256 Kbyte                |
| Embedded camera       | 99 x 72 YUV422 at 30 fps |
| Battery               | 320 mAh, 3.7 V           |
| Turning angular speed | $\approx 2\pi$ rad/s     |
| Low/High speeds       | $\approx 40/110$ mm/s    |
| Autonomy              | 1~2 hours                |

been modified to:

$$[W_{I_{off}}^k] = \frac{1}{8} \begin{bmatrix} 1 & 2 & 1 \\ 2 & 8 & 2 \\ 1 & 2 & 1 \end{bmatrix}. \quad (3)$$

After processing by the Medulla layer, the outputs from the ON/OFF channels are summed globally to obtain the membrane potential  $K_t$ . This potential is then passed through a sigmoid activation function to yield  $k_t$  [18]. To further enhance the model's selectivity, we introduce a spike frequency adaptation (SFA) mechanism formulated in [6]. The final output,  $\hat{k}_t$ , is then processed by the spike mechanism as follows:

$$S_t^{spike} = [e^{(\alpha \cdot (\hat{k}_t - T_{spi}))}]. \quad (4)$$

Here,  $\alpha$  is a scale parameter that influences the firing rate, and  $T_{spi}$  is the spike threshold. A collision is detected in a real-time robot experiment if  $n_{sp}$  spikes are generated within consecutive time steps, as defined by:

$$Col_t = \begin{cases} True, & \text{if } \sum_{i=t-n_{sp}}^t S_i^{spike} \geq n_{sp} \\ False, & \text{otherwise} \end{cases}. \quad (5)$$

The model parameters are relatively small in scale. Key parameters used in the model are listed in Table 1, while additional parameters can be found in [12].

## 2.2 Robot Configuration and Implementation

In this study, we applied the proposed composite neuronal model, in its two forms, to the ground-based mobile robot *Colias*, as illustrated in Figure 4. Due to its small size and low cost, *Colias* was used in swarm robotics research [1]. The robot is primarily composed of the Base Unit (CBU) and the Sense Unit (CSU), with relevant configurations detailed in Table 2. The CBU provides essential robot functions such as motion control, power management, and basic sensing. The CSU, which is mounted on top of the robot and houses the model, includes a main microprocessor and a compact camera. The top view of the CSU is shown in Figure 4. For more detailed information on the *Colias* robot, see [8].

**Processor** An ARM Cortex-M4F core microcontroller serves as the main processor, capable of handling extensive image processing and monitoring modules such as the camera and CSU. The 32-bit Micro Control Unit (MCU) STM32F427, equipped with 256KB SRAM and 2MB on-chip memory, operates at a high speed of 180MHz, contributing to both efficiency and low power consumption.

**Camera** The OV7670 module is a low-voltage CMOS image sensor capable of running at 30 frames per second with a resolution of  $72 \times 99$  pixels and a viewing angle of approximately 70 degrees, making it ideal for micro-robots.

**Implementation Strategy** Implementing the proposed model on this robot platform and ensuring real-time processing was a challenging task. To facilitate this, we used the ST-LINK (ST Microelectronics) to connect a computer with an Intel Core i7 processor to robot via a USB interface. The algorithms were then written and downloaded into Colias using the Keil uVision5 development tool. Given that the robot camera operates at a frame rate of 30 frames per second, the entire processing based on the proposed model must be completed within 33 milliseconds to maintain real-time performance.

To achieve this, we divided the computations of each cycle into eight phases (Ph1-Ph8), as depicted in Figure 3. In Module 1 (blue rectangular box), Ph1 computes the P layer from the original frame data. In Ph2, the Lamina layer is calculated, followed by Ph3, where the local S layer in the ON/OFF pathway and the I layer are computed. Ph4 then produces the output of Module 1. In Module 2 (pink rectangular box), the P layer is computed based on the output from Module 1. Ph6 and Ph7 are processed similarly to Ph2 and Ph3. Finally, Ph8 generates the final output to control robot motion. The entire online process is detailed in Algorithm 1. In our tests, the visual processing of each cycle took approximately 13 milliseconds, ensuring real-time processing.

### 2.3 Experimental Materials

As illustrated in Figure 4, the arena used in this research measured 1.4 meters in length and 0.8 meters in width, and was surrounded by LED-display walls decorated with static gratings. Within the arena, six cylindrical obstacles were positioned. A top-down camera was placed above the arena to record the robot's behavior. The robots' trajectories were tracked and analyzed by a localization system using ID-specific patterns, as described in [11].

## 3 Experiments and Results

This section presents the online robot experiments, which include both arena (closed-loop) tests and open-loop tests. The proposed composite neuronal model, implemented in two forms, was successfully applied in the robot's vision module. We compared its performance with two state-of-the-art collision perception models: the LGMD1-based model [6] and the LGMD2-based model [5].

---

**Algorithm 1:** Robot online implementation

---

```
Input: gray-scale luminance  $L(x, y, t)$ ,  $k \in \{1, 2\}$ 
1 while Power on do
2   if  $k = 1$  then
3     // LGMD1-LGMD2
4     Process  $L(x, y, t)$  with LGMD1 module;
5     Process LGMD1's output with LGMD2 module to obtain  $\hat{k}_t$ ;
6   else
7     // LGMD2-LGMD1
8     Process  $L(x, y, t)$  with LGMD2 module;
9     Process LGMD2's output with LGMD1 module to obtain  $\hat{k}_t$ ;
10    Calculate  $S_t^{spike}$  via Eq. (5) ;
11    Calculate  $Col_t$  via Eq. (6) ;
12    if  $col_t = True$  then
13      | Robot turns left or right;
14    else
15      | Robot goes forward;
16  end
17 end
```

---

**Table 3:** Success rate (%) of arena tests

| Case       | LGMD1-LGMD2 | LGMD2-LGMD1  | LGMD1 | LGMD2 |
|------------|-------------|--------------|-------|-------|
| low speed  | 92.6%       | <b>98.5%</b> | 90.9% | 97.0% |
| high speed | 90.2%       | <b>93.3%</b> | 78.8% | 89.4% |

### 3.1 Arena Tests

In the first type of robot experiment, we assessed the effectiveness and robustness of the proposed visual modality for guiding a ground mobile robot to detect and avoid collisions within an arena containing six obstacles. These tests aimed to compare the performance of the proposed composite LGMD neuronal model with the existing LGMD1 and LGMD2 models under controlled conditions. Each model was evaluated at two different speed settings: low and high (see Table 2 for details), with each experiment lasting 20 minutes. The *Colias* robot, equipped with each tested model, was initially programmed to move forward autonomously. Upon detecting a collision, the robot would turn left or right and then resume forward movement, repeating this process until the end of test.

Figure 5 illustrates the performance of the robot equipped with each visual modality across the two experimental sets. The statistical results for the success rate of collision avoidance in the arena tests are provided in Table 3. Overall, the results demonstrate that the composite model consistently outperformed the other models in both low- and high-speed scenarios, achieving higher suc-

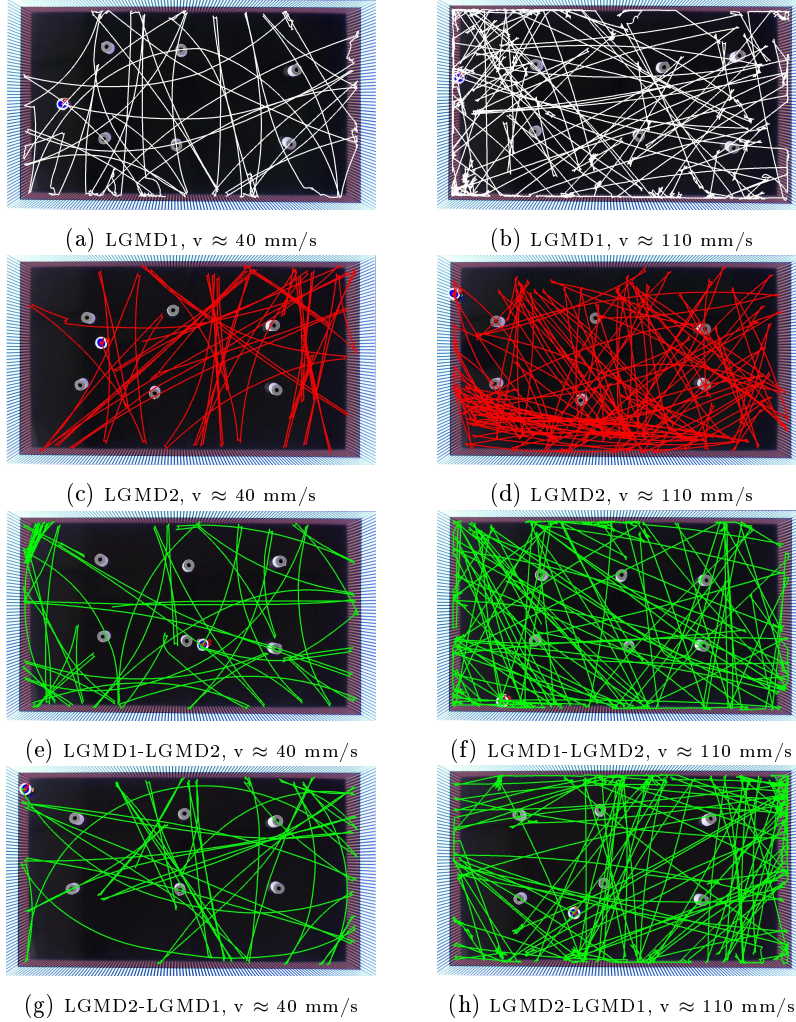


Fig. 5: The performance of the robot, equipped with each collision detection and avoidance model, was evaluated at two constant linear velocities within the arena. The trajectories over time were depicted for each model.

cess rates in collision detection and avoidance tasks within the arena. Notably, the LGMD2-LGMD1 configuration achieved the highest success rate in both experimental sets. Additionally, as the speed increased, the success rates of the LGMD1 and LGMD2 models declined significantly, whereas the two composite forms maintained stability even at high speeds. These arena tests not only confirmed the robustness and effectiveness of the proposed visual modality but also highlighted its capability to manage complex scenarios, such as detecting and avoiding rapidly approaching objects.

### 3.2 Open-loop Tests

In the second type of robot experiment, we employed four categorized motion patterns to stimulate the composite model and the comparison models. In these open-loop tests, the motion unit of the stimulated robot was deactivated, and we recorded its responses to visual stimuli generated by another moving robot.

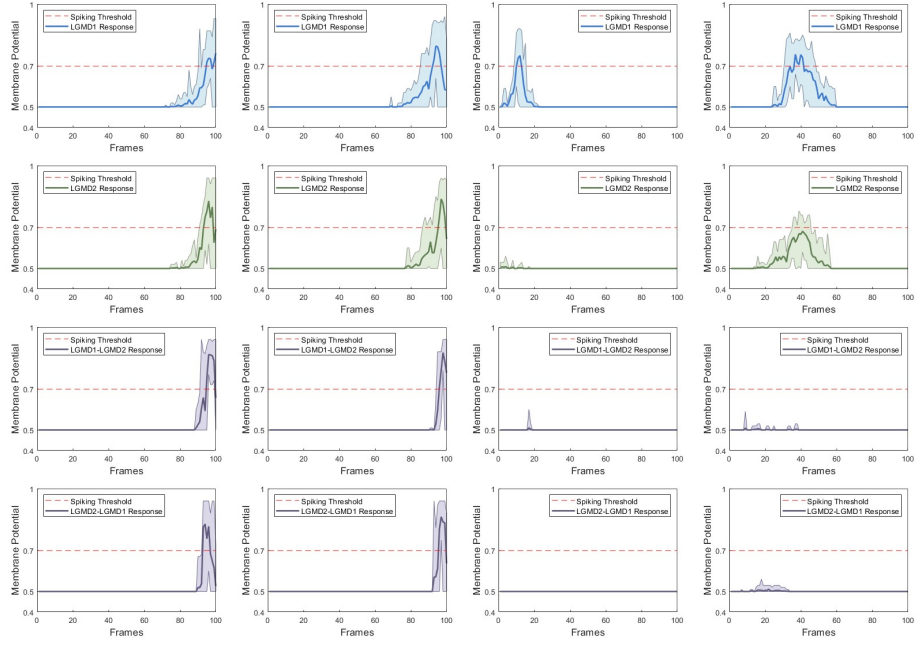


Fig. 6: Statistical outputs (membrane potential) and variance from repeated open-loop experiments with different models were recorded, stimulated by typical motion patterns. The data, presented from left to right in the columns, show how each model responds to frontal approaches at low speed (leftmost column) and high speed (middle-left), as well as receding at low speed (middle-right), and translating at low speed (rightmost column).

These experiments aimed to verify that the composite model, with its enhanced selectivity, is better suited for ground robots than the single-neuron models.

Figure 6 presents the statistical outputs of each model when challenged by typical motion patterns. Overall, the results highlight differences in activation and stability across the tested motion patterns. Specifically, both LGMD1 and LGMD2 exhibit strong responses to frontal approaches at both low and high speeds. LGMD1 shows brief responses to receding stimuli, whereas LGMD2 barely reacts to them. Although LGMD2 is slightly less responsive to translation compared to LGMD1, both models mistakenly identify translating stimuli as potential collisions. In contrast, the composite model, in both forms, is highly activated by frontal approaches while effectively inhibiting responses to receding and translating stimuli, with the LGMD2-LGMD1 form showing no response to receding at all. Notably, the variance in the composite model's responses is lower than that of the compared models. These findings underscore three key points: (1) The composite model is more stable than the compared models; (2) Compared to the single-neuron models, the composite model exhibits improved selectivity for looming stimuli, consistent with earlier findings [12]; and (3) The composite model shows promise as an embedded vision module for robots, making it particularly suitable for ground mobile robots detecting dark objects approaching.

## 4 Conclusions

In this paper, we proposed a bio-inspired embedded vision system for ground micro-robots to detect collisions by optimizing the computational complexity and memory usage of a composite LGMDs neuron model, ensuring both effectiveness and robustness. Compared to other embedded vision systems for collision detection, our system offers two key contributions: enhanced collision selectivity for approaching objects and improved stability in handling high-speed approaches. These advancements demonstrate the system's potential as a miniaturized visual modality for robots, enabling collision avoidance in dynamic, complex, and unpredictable environments. Looking ahead, we plan to further optimize memory usage to enhance the model and explore whether increasing the model's depth can improve its selectivity for looming stimuli.

## References

1. Arvin, F., Turgut, A.E., Krajiník, T., Yue, S.: Investigation of cue-based aggregation in static and dynamic environments with a mobile robot swarm. *Adaptive Behavior* **24**(2), 102–118 (2016)
2. DeSouza, G.N., Kak, A.C.: Vision for mobile robot navigation: A survey. *IEEE transactions on pattern analysis and machine intelligence* **24**(2), 237–267 (2002)
3. Franceschini, N.: Small brains, smart machines: from fly vision to robot vision and back again. *Proceedings of the IEEE* **102**(5), 751–781 (2014)
4. Fu, Q.: Motion perception based on on/off channels: a survey. *Neural Networks* **165**, 1–18 (2023)
5. Fu, Q., Hu, C., Peng, J., Rind, F.C., Yue, S.: A robust collision perception visual neural network with specific selectivity to darker objects. *IEEE transactions on cybernetics* **50**(12), 5074–5088 (2019)
6. Fu, Q., Hu, C., Peng, J., Yue, S.: Shaping the collision selectivity in a looming sensitive neuron model with parallel on and off pathways and spike frequency adaptation. *Neural Networks* **106**, 127–143 (2018)
7. Fu, Q., Wang, H., Hu, C., Yue, S.: Towards computational models and applications of insect visual systems for motion perception: A review. *Artificial Life* **25**(3), 263–311 (2019)
8. Hu, C., Fu, Q., Yue, S.: Colias iv: The affordable micro robot platform with bio-inspired vision. In: Annual Conference Towards Autonomous Robotic Systems. pp. 197–208. Springer (2018)
9. Iida, F., Lambrinos, D.: Navigation in an autonomous flying robot by using a biologically inspired visual odometer. In: Sensor fusion and decentralized control in robotic systems III. vol. 4196, pp. 86–97. SPIE (2000)
10. Indiveri, G., Douglas, R.: Neuromorphic vision sensors. *Science* **288**(5469), 1189–1190 (2000)
11. Krajiník, T., Nitsche, M., Faigl, J., Vaněk, P., Saska, M., Přeučil, L., Duckett, T., Mejail, M.: A practical multirobot localization system. *Journal of Intelligent & Robotic Systems* **76**, 539–562 (2014)
12. Li, J., Sun, X., Li, H., Peng, J., Fu, Q.: On the ensemble of collision perception neuron models towards ultra-selectivity. In: 2023 International Joint Conference on Neural Networks (IJCNN). pp. 1–8. IEEE (2023)

13. Rind, F.C., Bramwell, D.: Neural network based on the input organization of an identified neuron signaling impending collision. *Journal of neurophysiology* **75**(3), 967–985 (1996)
14. Roubieu, F.L., Serres, J.R., Colonnier, F., Franceschini, N., Viollet, S., Ruffier, F.: A biomimetic vision-based hovercraft accounts for bees' complex behaviour in various corridors. *Bioinspiration & Biomimetics* **9**(3), 036003 (2014)
15. Serres, J.R., Ruffier, F.: Optic flow-based collision-free strategies: From insects to robots. *Arthropod structure & development* **46**(5), 703–717 (2017)
16. Simmons, P.J., Rind, F.C.: Responses to object approach by a wide field visual neurone, the lgmd2 of the locust: characterization and image cues. *Journal of Comparative Physiology A* **180**, 203–214 (1997)
17. Sztarker, J., Rind, F.C.: A look into the cockpit of the developing locust: looming detectors and predator avoidance. *Developmental neurobiology* **74**(11), 1078–1095 (2014)
18. Yue, S., Rind, F.C.: Collision detection in complex dynamic scenes using an lgmd-based visual neural network with feature enhancement. *IEEE transactions on neural networks* **17**(3), 705–716 (2006)